Investigation of filamentary and diffuse DBD in CO 2 by means of in-situ FTIR absorption spectroscopy

Corentin Bajon, Edmond Baratte, Dihya Sadi, Olivier Guaitella, Antoine Belinger, Simon Dap, Tomas Hoder, Nicolas Naudé

Investigation of filamentary and diffuse DBD in CO_2 by means of *in-situ* FTIR absorption spectroscopy

C Bajon 1, E Baratte 2, D Sadi 2, O Guaitella 2, A Belinger 1, S Dap 1, T Hoder 3, N Naudé 1

1 LAPLACE, Université de Toulouse, CNRS, INPT, UPS, Toulouse, France

2 Laboratoire de Physique des Plasmas, Ecole Polytechnique, Route de Saclay, F-91128, Palaiseau Cedex, France

3 Department of Plasma Physics and Technology, Faculty of Science, Masaryk University, Kotlářská 2, 61137 Brno, Czech Republic

Abstract

This work investigates CO_2 dielectric barrier discharges at atmospheric pressure in the filamentary and diffuse regimes for the first time using *in situ* FTIR absorption measurements. The conversion factor of CO_2 is determined and is consistent with the results obtained for DBDs in the literature. Vibrational temperatures for CO_2 and CO molecules are also determined, as well as the rotational temperature. The ordering of the different temperatures is similar to the reported results for other CO_2 discharges. The evolution of the measured parameters as a function of the specific energy input is discussed and a comparison of the two different regimes is carried out.

Introduction

Interest in CO_2 plasmas started from the studies of CO_2 lasers in the 60's [1]. Further studies were dedicated to astrophysical observations [2,3] or to spacecraft shield design for atmosphere re-entry [4–6]. In the 70's, Fridman [7] and Capezzuto [8] were among the first to take advantage of the capability of non-equilibrium plasmas to induce chemistry in gases and to study the dissociation of CO_2 molecules. Non-equilibrium plasma discharges are an excellent way to produce oxygen from CO_2 during space missions [9–11], especially on Mars, where the atmosphere is composed of 95 % of CO_2. In addition, the current context, where global warming is a significant concern, motivates studies on CO_2 conversion into value-added products, for example, the production of methane from CO_2 and H_2 [12], or energy storage by the production of CO-H_2 "syngas" from CO_2 and CH_4, to reform hydrocarbons later [13,14]. Dielectric barrier discharges (DBDs) are interesting because they work at atmospheric pressure, are easy to set up, scalable and can be coupled with catalytic materials to improve CO_2 conversion. At this pressure, barrier discharges generally work in the well-known filamentary regime. However, it was demonstrated that obtaining a diffuse discharge in CO_2 at atmospheric pressure is possible as well [15]. This diffuse type of discharge works in the well-known atmospheric pressure Townsend regime (APTD), as it was initially reported in N_2 and later also in air [16–18]. In the Townsend regime, the electric field is almost constant along the gas gap [19,20]. It can be easily determined from the knowledge of the gas gap voltage, which can be determined by electrical measurements. This regime constitutes an exciting way to study the discharge mechanisms involved in CO_2 discharges because of the easy determination of the reduced electric field. In such APTD regime barrier discharge, it changes on relatively slow microsecond scales and peaks at low fields of approximately 120-140 Td, which represents another uniqueness in discharge conditions for CO_2 plasma study. Infrared absorption spectroscopy (FTIR) was used in low-pressure glow discharge [21–24], DBD [25] and recently in atmospheric pressure RF jets [26,27] to determine the dissociation rate of CO_2, and measure the energy distribution in the CO_2 and CO vibrational levels associated with their own temperature. The conversion rate of the CO_2 molecule into CO appears to be a function of the energy dissipated within the discharge. A non-equilibrium between the temperatures of the different vibrational modes of CO_2 was observed in the different discharge configurations, and a higher vibrational temperature of CO compared to vibrational temperatures of CO_2 was reported. In addition, the works of Morillo-Candas *et al.* [23,24] highlighted the importance of the CO(a) metastable and oxygen species, such as O_2 and atomic oxygen

in the discharge kinetic. In this work, *in-situ* FTIR absorption spectroscopy is used for the first time in CO_2 DBDs at atmospheric pressure in both diffuse (also referred as Townsend) and filamentary regimes. The results obtained for both regimes are then compared.

1. Experimental setup

The experimental setup used for this work is similar to the one used in [15]. The DBD cell, shown schematically in Figure 1a, was composed of two alumina plates 115x50 mm with a squared electrode of 3x3 cm painted on the outer side using a silver-based conductor painting (ESL 9916-G). The gas gap of 2 mm was set using four printed pieces, which maintain a glass plate to ensure a laminar gas flow. The glass plates were cut 5 mm before the electrode output allowing the IR beam to pass through the discharge.

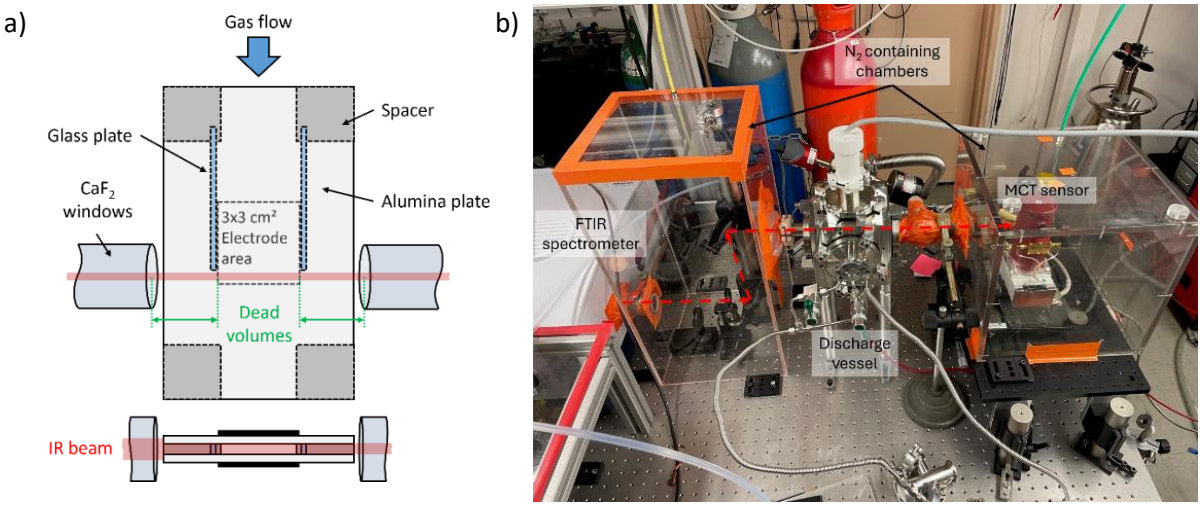

Figure 1: a) Top view diagram and b) picture of the experimental setup.

Before each experiment, the primary pump allows to reach a pressure of 10^{-3} mbar within the vessel. The vessel was filled with CO_2 Alphagaz 1 from Air Liquide©, with a purity of 99.999 %, for the experiments. The gas flow was set using a mass flow controller. An electronically controlled valve associated with a diaphragm pump was used to maintain a constant pressure of 1015 mbar during the experiments. The discharge cell was supplied by a low-frequency generator Keysight 33210A coupled to an audio amplifier connected to a high-voltage transformer. The applied voltage was measured using a Tektronix P6015A probe, and the current was measured through a shunt resistor placed in series with the discharge cell using a Rohde & Schwarz RT-ZP03 probe. Electrical characteristics were acquired using an oscilloscope Rohde & Schwarz RTB2004 with a bandwidth of 300 MHz. The discharge power was calculated by integrating the product of the measured voltage and current over one period. The gas voltage was determined from electrical measurements using an equivalent electrical circuit [28]. As the electric field is almost constant for a Townsend discharge, the electric field and then the reduced electric field E/N can be easily determined from the gas voltage, i.e. voltage over the gas gap (sometimes referred to as gap voltage).

The FTIR measurement setup was composed of a FTIR spectrometer Bruker V70 coupled with a MCT sensor cooled with liquid nitrogen. The IR beam of the spectrometer was guided through the discharge

cell by a set of mirrors and collected on the other side by the MCT sensor. The FTIR beam was collimated to pass through the gas gap. However, due to the large section of the IR beam, a part of it is cut, and only a fraction of the incident beam is collected by the MCT sensor. The absorption signal therefore corresponds to an average over the inter-electrode space, at the end of the plasma in the direction of the gas flow. At atmospheric pressure, the large amount of CO_2 molecules can be responsible for a total extinction of the IR beam in given spectral regions. To limit this saturation effect, the length of the optical path containing CO_2 was reduced using dedicated CaF_2 windows disposed as close as possible to the discharge cell (Figure 1a). In addition, the optical path from the FTIR spectrometer to the MCT sensor was purged with nitrogen circulation (see Figure 1b). Only the volume between the windows and the discharge area, called dead volume, contains pure CO_2 unexposed to the discharge. It must, therefore, be considered during the analysis of the absorption spectra. IR measurements were repeated for each condition until a steady state was reached.

Using the method described in [21], the IR spectra (Figure 2) were fitted to determine the vibrational temperatures of CO (T_{CO}) and CO_2 (T_{12} and T_3), the rotational temperature (T_{rot}) and the conversion factor α given in equation (1):

$$\alpha = \frac{[CO]}{[CO] + [CO_2]} \tag{1}$$

where $[CO]$ and $[CO_2]$ are the CO and CO_2 densities, respectively. The vibrational kinetic of the CO_2 molecule is described in [7]. The CO_2 molecule has three vibrational modes: a symmetric stretching mode ν_1, a double degenerate bending mode ν_2 and an asymmetric stretching mode ν_3 associated with the vibrational temperatures T_1, T_2 and T_3, respectively. The temperatures of the symmetric and bending modes of CO_2 are considered in Fermi equilibrium ($\hbar\nu_1 = 2\hbar\nu_2$), and consequently, a single temperature T_{12} is used to describe them. The temperature of the asymmetric mode T_3 is considered independently. A Treanor distribution is assumed for the population densities of the vibrational levels. The rotational temperature (T_{rot}) is assumed to be the same for all vibrational modes of CO_2 and CO. In the dead volumes, unlike in the plasma volume, the vibrational temperatures are assumed to be equal to T_{rot}, but the value of T_{rot} is not fixed. A similar gas composition is considered in both plasma volume and dead volume. The temperatures are determined with an error estimated to 30 K for CO_2 and around 100 K for CO using a sensitivity analysis by varying T_{rot}, T_{12}, T_3 and T_{CO} individually, as described in [21].

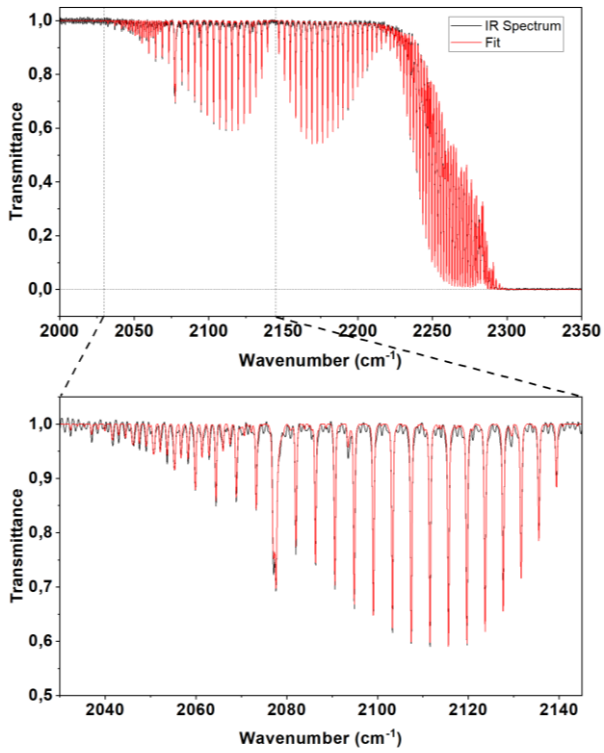

Figure 2: Example of a fitted IR spectrum. The IR spectrum is represented in black and the calculated spectrum in red (f = 2 kHz, V = 17 kVpp, gas gap = 2 mm, gas flow = 200 sccm).

2. Results and discussion

2.1. Specific energy input

This study investigates and compares the diffuse regime with a classical filamentary discharge regime. The frequency of the sine voltage is chosen as a parameter to switch from one discharge regime to the other. Indeed, for an amplitude of the applied voltage lower than 17 kV_{pp}, the discharge is systematically diffuse for a frequency of 1 kHz and filamentary for higher frequencies (2 kHz and 3 kHz). The influence of the amplitude of the applied voltage and the gas flow will be discussed later. The effect of all these parameters can considered using the specific energy input (SEI), which represents the amount of energy dissipated within a defined volume of gas during its interaction with the discharge. Then, many authors use SEI as a scaling parameter for CO conversion to compare discharges with different geometry, pressure, and electrical excitation [25,29–31]. The SEI is calculated using equation (2).

$$SEI = \frac{P}{\Phi}.\frac{p_0 T_g}{p T_0} = \frac{\tau \times P}{V} \quad (2)$$

with P the discharge power, Φ the gas flow injected through the discharge, p_0 and T_0 the standard conditions of pressure and temperature, T_g the gas temperature and p the experimental pressure. $\tau = \frac{V}{\Phi}$ is the residence time of the gas and V the volume of the discharge obtained by multiplying the area of the electrodes by the gas gap value.

To check the possible influence of the gas flow parameter on the dissipated plasma power in the discharge, we have conducted the following analysis. Figure 3a shows the discharge power as a function of the gas flow. For each excitation condition (frequency and amplitude of the applied voltage), the discharge power is almost independent of the gas flow in the explored range. It is worth mentioning that for an APTD generated in N_2 with small admixtures of oxidising gases such as O_2 (tens of ppm), some processes in the gas phase, such as associative ionisation reactions, occur [32]. Then, in N_2, a change in the gas flow rate while keeping the electrical parameters unchanged, induces a change in the discharge power. Whereas, in CO_2 APTD, the gas chemistry seems to have almost no influence. This is in good agreement with previous results provided in [15], where the memory effect was found to be independent of the species in the volume.

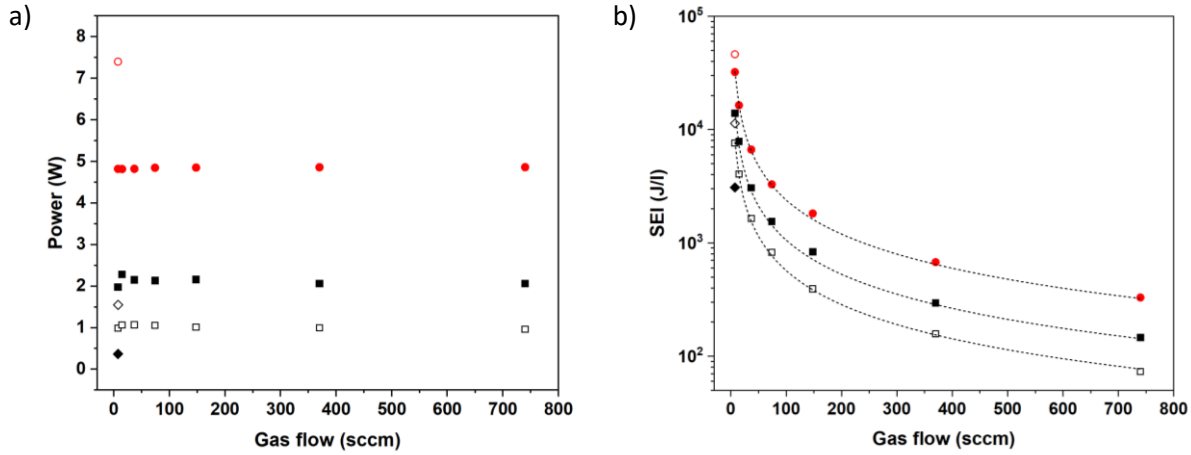

Figure 3: a) Discharge power and b) specific energy input (SEI) as a function of the gas flow for both diffuse regime (Townsend): black shapes (◆: 1 kHz 14 kV_{pp}, □: 1 kHz 15 kVpp, ◇: 1 kHz 16 kV_{pp}, ■: 1 kHz 17 kV_{pp}) and filamentary regime: red shapes (●: 2 kHz 17 kVpp and ○: 3 kHz 17 kV_{pp}).

The specific energy as a function of the gas flow for the different conditions of electrical excitation is represented in Figure 3b. SEI falls rapidly by two orders of magnitude when the gas flow increases from 7.4 sccm to 740 sccm, or residence time decreases from 14.6 s to 146 ms. The higher the gas flow, the lower the residence time of the gas and the lower the SEI for a similar electrical excitation condition. The moderate increase of the gas temperature with SEI (see section 2.3), as well as the independence of the discharge power regarding the gas flow, makes the SEI just inversely proportional to the gas flow. The SEI can thus be modified by changing the discharge power for a given gas flow, or by changing the gas flow for a given power, or by combining both approaches.

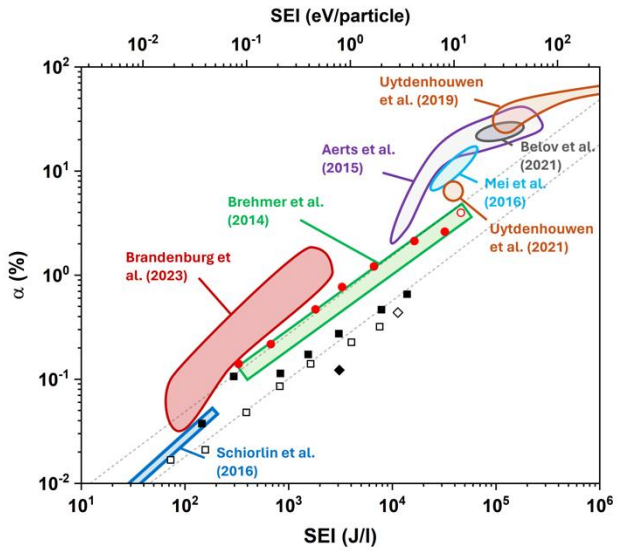

Figure 4: Conversion ratio α as a function of specific energy input (SEI). Our results were added to the figure reproduced from [29]. The dashed lines correspond to the fit of the experimental results obtained in the present work by imposing a slope of 0.75 for the diffuse regime (Townsend): black shapes (◆: 1 kHz 14 kV_{pp}, □: 1 kHz 15 kVpp, ◇: 1 kHz 16 kV_{pp}, ■: 1 kHz 17 kV_{pp}) and filamentary regime: red shapes (●: 2 kHz 17 kVpp and ○: 3 kHz 17 kV_{pp}).

2.2. CO_2 conversion factor

Figure 4 is reproduced from an article by Brandenburg *et al.* [29] and summarises the results obtained by different groups in CO_2 DBDs together with the results of this work. The conversion factor is shown as a function of the SEI. Red circles correspond to conditions for which the discharge works in the filamentary regime, whereas black squares are related to the diffuse discharge regime. The conversion ratio does not exceed a few percents, as it is reported in the literature for different barrier discharge configurations [33]. It is important to note that the discharge did not cover the whole electrode surface for the diffuse conditions at 14 kV_{pp} and 15 kV_{pp}. Then, the spreading of the discharge along the gas flow was estimated from the electrical measurements and imaging performed during additional dedicated measurements (see *e.g.* [34,35]). According to the obtained results, measurements at 15 kV_{pp} were still done within the discharge zone, whereas for the condition at 14 kV_{pp}, the measurements were done at the boundary between the discharge and the very beginning of the post-discharge. In the following, the SEI and residence time calculations were done considering the real discharge volume *i.e.* considering the spreading of the discharge. The values of α for the filamentary regime are in good agreement with the *ex-situ* measurements results obtained by Brehmer *et al.* [25] in atmospheric pressure DBD with quartz dielectrics and a gas gap of 1 mm (half of the gap used in this work). For a given SEI, the α factor is always higher for the filamentary regime than for the diffuse one. Indeed, it is now well accepted that in DBDs the CO_2 dissociation mainly occurs through direct electron impact with a low contribution of the vibrational ladder climbing [36]. Then, electrons with high energy in the tail of the energy distribution function play a significant role. The dissociation fraction results from a balance between the production and destruction of CO molecules. Considering that both regimes share rather similar conditions (pressure, nature of the surface, gas composition…) and assuming that the dominant production and destruction mechanisms are the same in both regimes (see discussion further), the lower dissociation degree observed in the diffuse regime could be explained by the lower reduced electric field values in this regime, which in turn is responsible for a lower population of energetic electrons. Indeed, E/N in the diffuse mode remains in the range 120-140

Td for all conditions, compared to the filamentary regimes where E/N values within the micro-discharges can reach values around 500 Td in the gas bulk [37,38]. Note that increasing the applied voltage in the Townsend regime (*i.e.* at a frequency of 1 kHz), does not result in an increase of the gas gap voltage, which remains close to the breakdown voltage, keeping unchanged the E/N value. Instead, it causes the discharge current and, thus, the electron density to increase, resulting in a slight increase of the discharge power (Figure 3) and thus of the dissociation fraction α (Figure 4). Conversion factor α grows when SEI increases. Both diffuse and filamentary results can be fitted by a straight line in log-log scale (which is similar to a power law in linear scale) *i.e.* $\alpha = k \times SEI^n$. A corresponding slope of $n = 0.67$ is found for both the filamentary and the diffuse regimes with R-squared values $R^2 = 0.99$ and $R^2 = 0.94$ respectively. Aerts *et al.* [39] have already shown using their numerical model that the conversion factor α in DBDs follows such a power law as a function of the SEI. In their review article, Brandenburg *et al.* [29] observed the same behaviour for SEI lower than 10 eV per particle by comparing the results of several works for different dielectric barrier discharge configurations. In his article Brehmer *et al.* reported a slope of $n = 0.75$ and developed a simple model considering the dissociation of CO_2 by collisions with electrons as a source term for CO production, and surface and volume recombination of CO as a loss term. If there are no losses, then $n = 1$, whereas including recombination losses leads to a lower value of the exponent. More recently, Douat *et al.* [30] reported a similar power law dependence with $n = 0.75$ for a discharge in pin-to-pin configuration at lower SEI. They attributed the power-law dependence to the fact that the number of filaments in filamentary DBDs also follows a power law. Nevertheless, the fact that this behaviour is also observed in purely diffuse DBD challenges this hypothesis and suggests that it is probably much more the result of a balance between gain and loss processes. Our value of the exponent $n = 0.67$ would thus suggest slightly higher CO losses than those of Brehmer and Douat, as discussed later. However, fitting our data by imposing $n = 0.75$ results in a good agreement for filamentary ($R^2 = 0.98$) and diffuse ($R^2 = 0.91$) regimes (see dashed lines on Figure 4). This shows that our results and the previously published ones remain close to each other. One of the possible explanations for this slight difference might be related to the lower number of measurements in our study.

The three-body recombination, see equation (3), is efficient only at high temperature or at the wall [36,40], equation (4) (in this case, M represents the wall itself).

$$CO + O + M \rightarrow CO_2 + M \quad (3)$$

$$CO + O + wall \rightarrow CO_2 + wall \quad (4)$$

In our conditions, the gas temperature remains moderate (see [28] and next part), thus if this reaction plays a role, it will likely occur at the surface. The rate of wall recombination is difficult to assess but one can estimate the characteristic diffusion time τ_{diff} of O and CO to the walls and the associated frequency. Due to the small gas gap compared to the dimension of the system, τ_{diff} can be approximated to $\tau_{diff} = \frac{d^2}{\pi^2 D}$ where $d = 2mm$ is the gap length and D the diffusion coefficient of the specie of interest. Morillo-Candas *et al.* [41] reported two different diffusion coefficients for atomic oxygen, coming from Cenian *et al.* [42] and Klarenaar *et al.* [22]. Under our conditions, τ_{diff} for O atoms is in the range of 9 – 15 ms using the diffusion coefficient from Cenian, and 2 times larger according to Klarenaar. For CO, estimated τ_{diff} ranges between 18 and 28 ms where the diffusion coefficient of CO was calculated according to [43]. These values are well below the lower value of the residence time τ in our conditions which is about 140 ms. It means that particles have enough time to reach the surface by diffusion during their stay within the gas flow. Brehmer *et al.* used coefficient rates from [42] to study the backreaction mechanisms in gas phase, see equation (3), and at the surfaces, eq. (4), and reported a similar rate coefficient $k \approx 1.5 \times 10^{-15}$ $cm^3\ s^{-1}$. Our results are comparable to

[25] in terms of α, gap length and gas temperature (see next section). Therefore, we assume a similar coefficient rate for both reaction mechanisms. Considering only these backreaction mechanisms as CO loss channels is consistent with behaviour similar to that observed by Brehmer *et al.*. Note that also other mechanisms are suspected to be of major importance in the backreactions mechanisms in CO_2 plasmas, such as the metastable species $O(^1D)$ or $CO(a^3\Pi)$, which could react with CO and/or O_2 to form CO_2 again, or O_2 ($a^1\Delta_g$) and $O_2(b^1\Sigma^+_g)$ [36]. Despite an impossible estimation of their contribution with the available data, the fact that the slope of the $\alpha = f(SEI)$ curve is the same for both discharge regimes suggests that the dominant mechanisms are the same whether they are gain or loss processes, and that their relative importance does not strongly vary with the E/N value in the range covered by the present study.

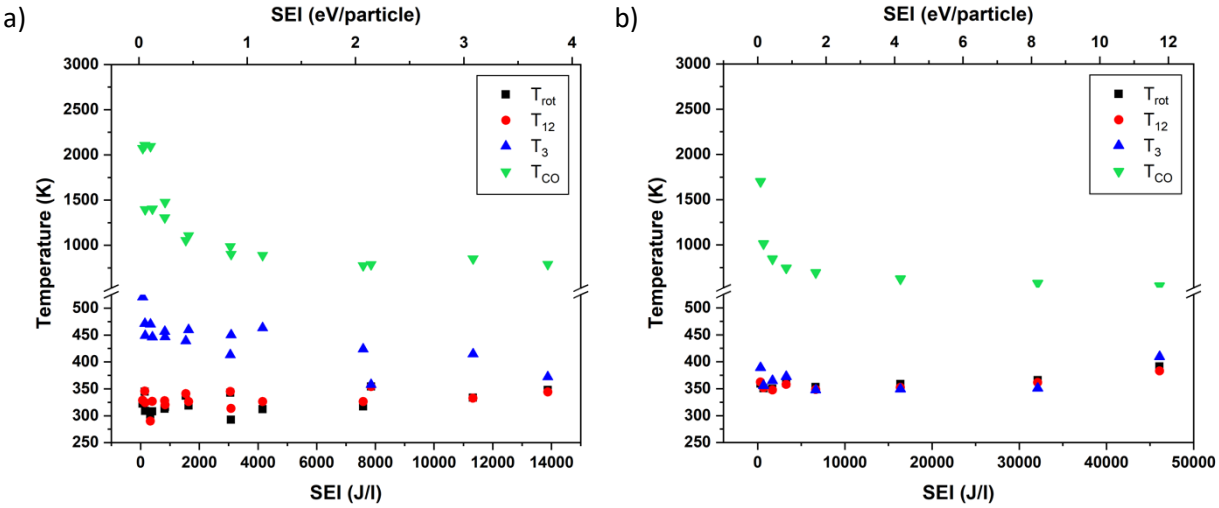

Figure 5: Rotational temperature (T_{rot}: ■) and vibrational temperature of CO_2 and CO (T_{12}: ▲, T_3: ● and T_{CO}: ▲) as a function of the SEI in a) Diffuse regime (Townsend) and b) filamentary regime.

2.3. Vibrational kinetic

As explained in section 1, due to the Fermi resonance between ν_1 and ν_2, important energy transfers occur between these two modes, which are thus strongly coupled and can be considered as a triple degenerate mode associated with a single vibrational temperature denoted hereafter as T_{12}. The CO molecule has only one vibration mode associated with temperature T_{CO}. Figure 5 shows the rotational temperature T_{rot}, the vibrational temperature of the symmetric-bending mode of CO_2 (T_{12}), the vibrational temperature of the asymmetric mode of CO_2 (T_3) and the vibrational temperature of CO (T_{CO}) obtained for both studied discharge regimes. Let us first discuss the results obtained for the diffuse regime (Figure 5a), whereas the results obtained for the filamentary regime (Figure 5b) will be discussed at the end of this section.

The general ordering of the different temperatures: $T_{CO} > T_3 > T_{12} \approx T_{rot}$ is consistent with the results reported in several works [36,44] except that under our conditions, the difference between T_{CO} and T_3 is very large, with T_{CO} being at least 500 K higher. Due to the short energy gap between the vibrational levels of symmetric stretching and bending modes of CO_2, the V-T relaxation mechanisms are efficient. The energy of the vibrational levels ν_1 and ν_2 is thus easily lost in gas heating, and consequently, T_{12} remains close to T_{rot}. On the contrary, the energy gap between the vibrational levels of the asymmetric mode is larger, and thus, the V-T relaxation mechanisms are less efficient. This

difference results in a non-equilibrium between symmetric-bending mode (T_{12}) and asymmetric stretching mode (T_3). This non-equilibrium is generally favoured by the resonance between the vibrational level of CO and the asymmetric stretching mode of CO_2, which can result in vibrational energy transfer from CO to the v_3 mode of CO_2. Nevertheless, in our conditions, the dissociation fraction is too low for these energy transfers to significantly contribute to a rise of T_3. This is especially true for low SEI for which T_{CO} exceeds T_3 by more than 2000 K in the diffuse regime and can at least partly explain why T_{CO}>>T_3. Energy stored in the different vibrational modes can be estimated by the product $\varepsilon = nk_BT$, where n is the density of CO_2 or CO, k_B the Boltzmann constant and T the temperature associated to the vibrational mode under study. Corresponding results are represented in Figure 6 for diffuse and filamentary regimes. Note that here $\varepsilon_{12} = 2 \times n_{CO_2} k_B T_{12}$. It is clearly visible that the energy of the CO vibrations is very low regarding to the CO_2 vibrational modes. Indeed, ε_{CO} represents less than 1 % of the total vibrational energy. It confirms that even if there is a resonance between CO and the asymmetric mode of CO_2, the amount of energy stored in the vibrational modes of CO is too low to significantly impact T_3. Other phenomena can also be responsible for this large difference between T_3 and T_{CO}. Vibrational intermodal exchanges occur between the asymmetric mode of CO_2 and the symmetric stretching and bending modes (V-V' exchanges), while these V-V' exchanges do not exist for the CO molecule. Also, according to [23], the V-T relaxation processes are slightly more efficient for the v_3 mode of CO_2 compared to CO, whereas vibrational excitation by collision with electronically excited species as CO($a^3\Pi$) and O(^1D), which are products of the CO_2 dissociation by direct electron impact, could be more efficient for CO. Fromentin *et al.* [44] also reported an unusually large cross section for the excitation of the vibrational levels of CO which is related to a resonance effect with short-lived negative ions CO^- [45]. In conclusion, the higher value of T_{CO} compared to T_3 probably results from a combination of several mechanisms, including: 1) limited vibrational energy transfer from CO to CO_2, 2) V-V' transfers and higher VT relaxation for v_3 compared to CO and 3) higher energy transfers towards the vibrational levels of CO.

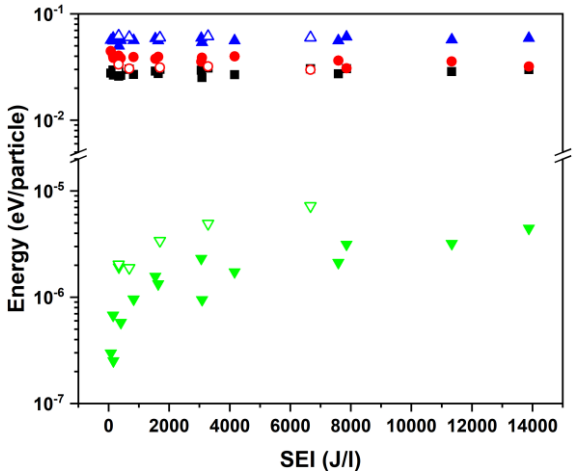

Figure 6: Energies associated to the vibrational temperatures T_{rot}: ■, T_{12}: ▲, T_3: ● and T_{CO}: ▲ as a function of the SEI for diffuse regime (filled shapes) and filamentary regime (empty shapes).

Another interesting phenomenon is the evolution of the temperatures with the SEI, and especially T_{CO}. The trends are similar for both regimes. As SEI increases, T_{CO} rapidly decreases. In the diffuse regime, it drops from 2073 K at 73 J/l to 986 K at 3058 J/l. The decrease is less pronounced for T_3. Indeed, on the same range of SEI, it only decreases from 520 K to 413 K. Whereas T_{12} only slightly increases from

room temperature (300 K) for the lower SEI to 348 K for 13877 J/l. Having in mind that the dissociation fraction α in both regimes is different, it is interesting to have a look at the evolution of the temperatures as a function of α. Figure 7 shows the evolution of T_{CO} with α. All the experimental data for both regimes are aligned on the same curve, indicating that α is a relevant parameter and suggesting that the dissociation products O and/or CO can play a role in this evolution. Atomic oxygen is known to be a good quencher of vibrational levels and the V-T relaxations of CO_2 and CO molecules by collision with O atoms are dominant [23]. Figure 8 shows the quenching frequencies of the vibrational levels of CO and CO_2 (ν_2 and ν_3) by O atoms as a function of α. These frequencies were determined by multiplying the quenching rate coefficient k taken from the literature [23,44] by the density of O atoms, which is estimated from the dissociation fraction using the ideal gas law and the measured rotational temperature. The O atoms density was considered equal to the CO density, thus neglecting recombination. In this way, atomic oxygen density is overestimated, and the computation provides an upper limit of the quenching rate. V-T relaxation rate by CO_2, which is the dominant species within the discharge, is added for direct comparison. The quenching rate coefficient of CO_2 symmetric and asymmetric stretching modes were found in [23,44] from the work of [46–48]. The rate coefficient for the quenching of CO($v = 1$) by collision with O atoms came from [49] and the rate coefficient for V-T relaxation of CO(v) through collisions with CO_2 was obtained using the same method as described in [44]. Due to the large number of CO_2 molecules in our conditions (low dissociation rate), deexcitation frequencies of CO_2 by collision with another CO_2 molecule are almost constant independently of the conversion factor. The calculated quenching frequencies by O atoms increase rapidly for low values of α with the apparition of CO and O. The results clearly show that V-T processes of CO are dominated by collisions with O atoms. The deexcitation frequency is thus directly related to the O atom density. It is thus reasonable to assume that for very low SEI, the appearance of O atoms in the discharge is responsible for a significant increase of the VT processes of CO, leading to the observed drop of T_{CO} in the diffuse and filamentary regimes. In addition, due to the large amount of CO_2, V-T relaxations of CO_2 vibrations by collision with another CO_2 molecule are efficient, which could explain why T_3 and T_{12} remain low whatever the dissociation degree. A large difference between the vibrational temperatures of CO and the asymmetric mode of CO_2 was also observed in noble gases with an admixture of CO_2 [26,27]. In these works, the dilution of CO_2 into noble gas limits the transfer between T_{CO} and T_3 as it is in our conditions due to the low amount of CO. It also reduces the quenching rate of CO vibrations by atomic oxygen.

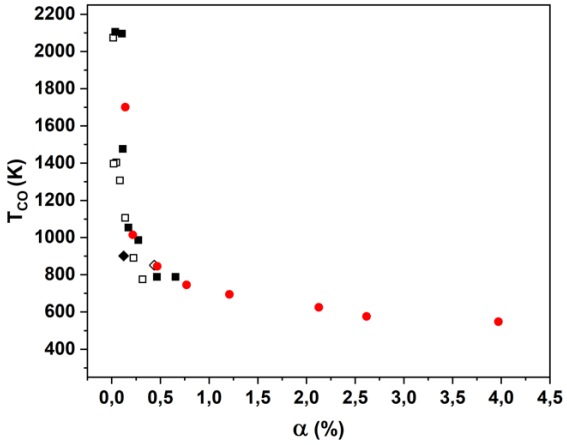

Figure 7: Vibrational temperature of CO as a function of α. Diffuse regime (Townsend): black shapes (◆: 1 kHz 14 kV_{pp}, □: 1 kHz 15 kVpp, ◇: 1 kHz 16 kV_{pp}, ■: 1 kHz 17 kV_{pp}) and filamentary regime: red shapes (●: 2 kHz 17 kVpp and ○: 3 kHz 17 kV_{pp}).

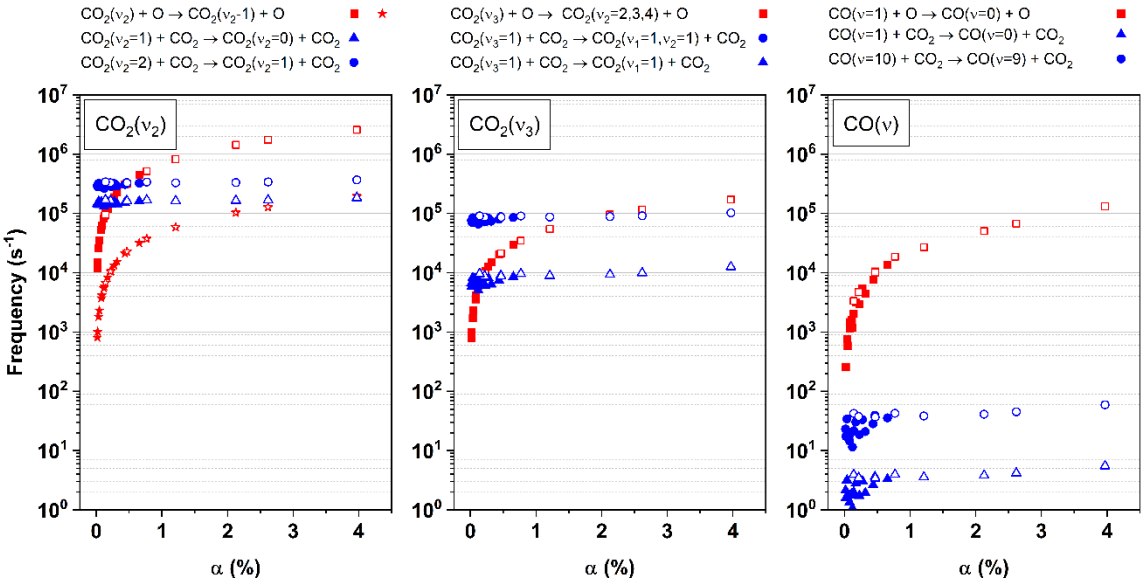

Figure 8: V-T relaxation frequencies of the vibrational levels of CO_2(v_2 and v_3) and CO(v) by collision with O and CO_2 as a function of α. Diffuse regime (Townsend) corresponds to filled shapes and filamentary regime is associated to empty shapes. The reactions involving atomic oxygen are represented in red and those involving CO_2 molecule as collision partner are in blue. Two different reaction rates, coming from [23] (■) and [44] (★), were used for the calculation of the V-T frequencies by collision with O for the symmetric bending mode (v_2).

In the filamentary regime (Figure 5b), the main difference with the results obtained in the diffuse regime concerns T_3 which is equal to T_{12} and T_{rot}. The general ordering becomes $T_{CO} > T_3 \approx T_{12} \approx T_{rot}$. Note that in addition for a given SEI, T_{CO} is systematically lower compared to the diffuse regime (from 300 K at lower SEI to 150 K i.e. above the error bar). One of the possible explanations is related to the measurement technique itself. Indeed, FTIR absorption measurements are integrated over space (along the beam path and the width of the beam) and over time. The filamentary discharge being made of numerous plasma filaments randomly distributed in time and space, an average is done during the measurements between the gas contained within the filaments and the cold gas located around. Another hypothesis is that in the filamentary regime, the dissociation of CO_2 molecules occurs within the volume of a plasma filament, which means that the local density of the dissociation products can reach high values during the filament lifetime. The aforementioned V-T processes related *e.g.* to oxygen atoms can thus be significantly higher compared to the diffuse discharge, explaining both the lower T_{CO} and T_3 even for very small SEI. This V-T processes probably also plays a role in the diffuse regime but to a lower extent: T_3 continuously decreases when increasing the SEI and approaches the value of T_{12} only for the largest SEI investigated. As a conclusion, the observed equilibrium between T_3, T_{12} and T_{rot} in the filamentary regime probably results both from an averaging effect during the measurement and from strong V-T energy transfers due to a high O atoms density within the plasma filaments.

To go further in this discussion, an accurate determination of the O atom density is thus necessary as well as the use of a detailed modelling of the vibrational kinetics.

3. Summary and conclusion

In-situ FTIR measurements were performed in pure CO_2 DBD at atmospheric pressure in the diffuse and filamentary regimes. The results were analysed to get the dissociation fraction and the vibrational

excitation of CO_2 and CO through the determination of the vibrational temperatures T_3, T_{12} and T_{CO} of the CO_2 and CO molecules, respectively. The dissociation fraction follows a power law with respect to the specific energy input (SEI) with an exponent of 0.67 for both the diffuse and the filamentary regimes. It is close to value of 0.75 already published in the literature [25,30]. This power law is probably the result of the complex chemistry taking place in CO_2 discharges. The maximum conversion rate in the investigated range of specific energy input (SEI) was about 4% at 46 000 J/l (≈10 eV/particle). For a given SEI, the dissociation was found to be more efficient in the filamentary regime, probably due to higher values of the reduced electric field. In the diffuse regime, the ordering of the different temperatures is similar to what has already been reported in the literature: $T_{CO} > T_3 > T_{12} \approx T_{rot}$. Nevertheless, we observed an unexpectedly significant difference between T_3 and the temperature T_{CO}. Part of the explanation probably relies on the low density of CO molecules limiting the transfer between vibrations of CO and the asymmetric mode of CO_2. In addition, a significant drop of T_{CO} with SEI was observed for low SEI values in both discharge regimes, which was attributed to VT transfers with oxygen atoms. Surprisingly in the filamentary regime, T_3 is found to be equal to T_{12} over the whole range of SEI investigated. It can result from an averaging effect between the excited gas within the plasma filaments and the surrounding cold gas during the absorption measurements and to strong VT transfers in the filaments due to the higher density of O atoms. To go further, the possible role played by ground state and excited species, such as CO($a^3\Pi$) or metastable states of molecular oxygen, would require a numerical model to be investigated. In addition, the determination of the O atoms density would be beneficial to definitely validate the aforementioned hypothesis, which will be the topic of future work.

[1] Witteman W J 2013 *CO2 Laser* (S.l.: Springer Berlin Heidelberg)

[2] D'Hendecourt L B and Jourdain de Muizon M 1989 The discovery of interstellar carbon dioxide. *Astronomy and Astrophysics* **223** L5–8

[3] Wyckoff S and Theobald J 1989 Molecular ions in comets *Advances in Space Research* **9** 157–61

[4] Herdrich G, Auweter-Kurtz M, Kurtz H L, Laux T and Winter M 2002 Operational Behavior of Inductively Heated Plasma Source IPG3 for Entry Simulations *Journal of Thermophysics and Heat Transfer* **16** 440–9

[5] Vacher D, Lino da Silva M, André P, Faure G and Dudeck M 2008 Radiation from an equilibrium CO_2–N_2 plasma in the [250–850 nm] spectral region: I. Experiment *Plasma Sources Science and Technology* **17** 035012

[6] Lin X, Chen L Z, Li J P, Li F and Yu X L 2018 Experimental and Numerical Study of Carbon-Dioxide Dissociation for Mars Atmospheric Entry *Journal of Thermophysics and Heat Transfer* **32** 503–13

[7] Fridman A A 2008 *Plasma chemistry* (Cambridge University Press)

[8] Capezzuto P, Cramarossa F, D'Agostino R and Molinari E 1976 Contribution of vibrational excitation to the rate of carbon dioxide dissociation in electrical discharges *The Journal of Physical Chemistry* **80** 882–8

[9] Guerra V, Silva T, Ogloblina P, Grofulović M, Terraz L, Silva M L D, Pintassilgo C D, Alves L L and Guaitella O 2017 The case for in situ resource utilisation for oxygen production on Mars by non-equilibrium plasmas *Plasma Sources Science and Technology* **26**

[10] Premathilake D, Outlaw R A, Quinlan R A and Byvik C E 2019 Oxygen Generation by Carbon Dioxide Glow Discharge and Separation by Permeation Through Ultrathin Silver Membranes *Earth and Space Science* **6** 557–64

[11] Ogloblina P, Morillo-Candas A S, Silva A F, Silva T, Tejero-Del-Caz A, Alves L L, Guaitella O and Guerra V 2021 Mars in situ oxygen and propellant production by non-equilibrium plasmas *Plasma Sources Science and Technology* **30**

[12] Sivachandiran L, Costa P D and Khacef A 2020 CO2 reforming in CH4 over Ni/γ-Al2O3 nano catalyst: Effect of cold plasma surface discharge *Applied Surface Science* **501** 144175

[13] Ozkan A, Dufour T, Arnoult G, De Keyzer P, Bogaerts A and Reniers F 2015 CO2–CH4 conversion and syngas formation at atmospheric pressure using a multi-electrode dielectric barrier discharge *Journal of CO2 Utilization* **9** 74–81

[14] Bogaerts A, De Bie C, Snoeckx R and Kozák T 2017 Plasma based CO_2 and CH_4 conversion: A modeling perspective *Plasma Processes and Polymers* **14** 1600070

[15] Bajon C, Dap S, Belinger A, Guaitella O, Hoder T and Naudé N 2023 Homogeneous dielectric barrier discharge in CO_2 *Plasma Sources Science and Technology* **32** 045012

[16] Massines F, Gherardi N, Naudé N and Ségur P 2005 Glow and Townsend dielectric barrier discharge in various atmosphere *Plasma Physics and Controlled Fusion* **47** B577–88

[17] Osawa N, Takashi A, Yoshioka Y and Hanaoka R 2013 Generation of high pressure homogeneous dielectric barrier discharge in air *The European Physical Journal Applied Physics* **61** 24317

[18] Tyl C, Lin X, Bouzidi M C, Dap S, Caquineau H, Ségur P, Gherardi N and Naudé N 2018 Investigation of memory effect in atmospheric pressure dielectric barrier discharge in nitrogen with small oxygen or nitric oxide addition *Journal of Physics D: Applied Physics* **51**

[19] Mrkvic M 2023 Electric field in APTD in nitrogen determined by EFISH, FNS/SPS ratio, α-fitting and electrical equivalent circuit model *Plasma Sources Sci. Technol.*

[20] Massines F, Ségur P, Gherardi N, Khamphan C and Ricard A 2003 Physics and chemistry in a glow dielectric barrier discharge at atmospheric pressure: diagnostics and modelling *Surface and Coatings Technology* **174–175** 8–14

[21] Klarenaar B L M, Engeln R, van den Bekerom D C M, van de Sanden M C M, Morillo-Candas A S and Guaitella O 2017 Time evolution of vibrational temperatures in a CO_2 glow discharge measured with infrared absorption spectroscopy *Plasma Sources Science and Technology* **26** 115008

[22] Klarenaar B L M, Morillo-Candas A S, Grofulović M, Sanden M C M van de, Engeln R and Guaitella O 2019 Excitation and relaxation of the asymmetric stretch mode of CO_2 in a pulsed glow discharge *Plasma Sources Science and Technology* **28** 035011

[23] Morillo-Candas A S, Klarenaar B L M, Amoedo C, Guerra V and Guaitella O 2020 Effect of oxygen atoms on the vibrational kinetics of CO2and CO revealed by the use of a large surface area material *Journal of Physics D: Applied Physics* **54**

[24] Morillo-Candas A S, Guerra V and Guaitella O 2020 Time Evolution of the Dissociation Fraction in rf CO2Plasmas: Impact and Nature of Back-Reaction Mechanisms *Journal of Physical Chemistry C* **124** 17459–75

[25] Brehmer F, Welzel S, Van De Sanden M C M and Engeln R 2014 CO and byproduct formation during CO2 reduction in dielectric barrier discharges *Journal of Applied Physics* **116**

[26] Urbanietz T, Böke M, Schulz-von der Gathen V and von Keudell A 2018 Non-equilibrium excitation of CO_2 in an atmospheric pressure helium plasma jet *Journal of Physics D: Applied Physics* **51** 345202

[27] Stewig C, Schüttler S, Urbanietz T, Böke M and von Keudell A 2020 Excitation and dissociation of CO_2 heavily diluted in noble gas atmospheric pressure plasma *Journal of Physics D: Applied Physics* **53** 125205

[28] Naudé N, Cambronne J-P, Gherardi N and Massines F 2005 Electrical model and analysis of the transition from an atmospheric pressure Townsend discharge to a filamentary discharge *Journal of Physics D: Applied Physics* **38** 530–8

[29] Brandenburg R, Schiorlin M, Schmidt M, Höft H, Pipa A V and Brüser V 2023 Plane Parallel Barrier Discharges for Carbon Dioxide Splitting: Influence of Discharge Arrangement on Carbon Monoxide Formation *Plasma* **6** 162–80

[30] Douat C, Ponduri S, Boumans T, Guaitella O, Welzel S, Carbone E and Engeln R 2023 The role of the number of filaments in the dissociation of CO_2 in dielectric barrier discharges *Plasma Sources Science and Technology* **32** 055001

[31] Salden A, Budde M, Garcia-Soto C A, Biondo O, Barauna J, Faedda M, Musig B, Fromentin C, Nguyen-Quang M, Philpott H, Hasrack G, Aceto D, Cai Y, Jury F A, Bogaerts A, Da Costa P, Engeln R, Gálvez M E, Gans T, Garcia T, Guerra V, Henriques C, Motak M, Navarro M V, Parvulescu V I, Van Rooij G, Samojeden B, Sobota A, Tosi P, Tu X and Guaitella O 2023 Meta-analysis of CO2 conversion, energy efficiency, and other performance data of plasma-catalysis reactors with the open access PIONEER database *Journal of Energy Chemistry* **86** 318–42

[32] Lin X, Tyl C, Naudé N, Gherardi N, Popov N A and Dap S 2020 The role of associative ionization reactions in the memory effect of atmospheric pressure Townsend discharges in N_2 with a small O_2 addition *Journal of Physics D: Applied Physics* **53** 205201

[33] Snoeckx R and Bogaerts A 2017 Plasma technology-a novel solution for CO2 conversion?

[34] Tyl C, Martin S, Combettes C, Brillat G, Bley V, Belinger A, Dap S, Brandenburg R and Naudé N 2021 New local electrical diagnostic tool for dielectric barrier discharge (DBD) *Review of Scientific Instruments* **92** 053552

[35] Belinger A, Dap S and Naudé N 2022 Influence of the dielectric thickness on the homogeneity of a diffuse dielectric barrier discharge in air *J. Phys. D: Appl. Phys.* **55** 465201

[36] Pietanza L D, Guaitella O, Aquilanti V, Armenise I, Bogaerts A, Capitelli M, Colonna G, Guerra V, Engeln R, Kustova E, Lombardi A, Palazzetti F and Silva T 2021 Advances in non-equilibrium CO 2 plasma kinetics: a theoretical and experimental review

[37] Ponduri S, Becker M M, Welzel S, Van De Sanden M C M, Loffhagen D and Engeln R 2016 Fluid modelling of CO2 dissociation in a dielectric barrier discharge *Journal of Applied Physics* **119**

[38] Jánský J, Bessiéres D, Brandenburg R, Paillol J and Hoder T 2021 Electric field development in positive and negative streamers on dielectric surface *Plasma Sources Science and Technology* **30** 105008

[39] Aerts R, Somers W and Bogaerts A 2015 Carbon Dioxide Splitting in a Dielectric Barrier Discharge Plasma: A Combined Experimental and Computational Study *ChemSusChem* **8** 702–16

[40] Otorbaev D K 1995 Catalytic properties of surfaces with respect to generation of CO2 molecules in the plasma *Chemical Physics* **196** 543–50

[41] Morillo-Candas A S, Drag C, Booth J P, Dias T C, Guerra V and Guaitella O 2019 Oxygen atom kinetics in CO2 plasmas ignited in a DC glow discharge *Plasma Sources Science and Technology* **28**

[42] Cenian A, Chernukho A, Borodin V and Śliwiński G 1994 Modeling of Plasma-Chemical Reactions in Gas Mixture of CO2 Lasers I. Gas Decomposition in Pure CO2 Glow Discharge *Contributions to Plasma Physics* **34** 25–37

[43] Bird R B, Stewart W E and Lightfoot E N 2007 *Transport phenomena* (New York: Wiley)

[44] Fromentin C, Silva T, Dias T C, Morillo-Candas A S, Biondo O, Guaitella O and Guerra V 2023 Study of vibrational kinetics of CO_2 and CO in CO_2–O_2 plasmas under non-equilibrium conditions *Plasma Sources Science and Technology* **32** 024001

[45] Ehrhardt H, Langhans L, Linder F and Taylor H S 1968 Resonance Scattering of Slow Electrons from H 2 and CO Angular Distributions *Physical Review* **173** 222–30

[46] Lopez-Puertas M and Taylor F W 2001 *Non-LTE radiative transfer in the atmosphere* (Singapore: World Scientific Publ. Co)

[47] López-Puertas M, Rodrigo R, Molina A and Taylor F W 1986 A non-LTE radiative transfer model for infrared bands in the middle atmosphere. I. Theoretical basis and application to CO2 15 μm bands *Journal of Atmospheric and Terrestrial Physics* **48** 729–48

[48] Blauer J and Nickerson G 1974 A survey of vibrational relaxation rate data for processes importantto CO2-N2-H2O infrared plume radiation *7th Fluid and PlasmaDynamics Conference* 7th Fluid and PlasmaDynamics Conference (Palo Alto,CA,U.S.A.: American Institute of Aeronautics and Astronautics)

[49] Capitelli M, Ferreira C M, Gordiets B F and Osipov A I 2000 *Plasma Kinetics in Atmospheric Gases*